

<https://doi.org/10.1038/s40494-026-02356-3>

Inspiration from Chinese paintings of Song Dynasty: the influence of the traditional architectural component Yinyan on indoor wind environments

Check for updates

Hua Zhang ¹, Minghui Xiong ¹ ✉, Bing Chen ² ✉, Kaiguo Si¹ & Jialong Lai ³

This paper explores the impact of “Yinyan”, a climate-responsive building component depicted in the paintings of the Song Dynasty (960–1279 AD), on indoor wind environments, aiming to support the digital representation and multisensory simulation of architectural heritage. Although few buildings from the Song Dynasty remain, Song paintings, renowned for their realism, provide detailed visual records that can inform the representation of the then buildings. In this study, a building depicted in the *Life along the Bian River at the Qing Ming Festival (Qing Ming Shang He Tu in Pinyin)* was modeled according to the Song construction manual – *Yingzao Fashi*. Numerical simulation was then conducted to evaluate the impact of “Yinyan”, given its various designs, on indoor wind environments. The results provide scientific evidence for the multisensory digital representation of architectural heritage from the Song Dynasty, and offer insights for their conservation and restoration as well as for sustainable building designs nowadays.

The rapid advancement of digital technologies has profoundly transformed the conservation, dissemination, and education of architectural heritage^{1–3}. Digital tools such as Virtual Reality (VR) and Augmented Reality (AR) have overcome the spatial and temporal limitations of traditional heritage education, enhancing public engagement and improving the effectiveness of cultural transmission^{4–6}. Built on this, multi-sensory digital heritage has emerged as a new and important research field, where the accuracy of details is critical for effective multi-sensory digital representation. This is particularly important for climate-adaptive building components in architectural heritage, as they are closely related to human perception. Inaccurate representations may undermine the design wisdom embedded in historical architecture and weaken the scientific value of heritage education. The Song Dynasty (960–1279 AD) was a remarkable period in the history of Chinese architecture, characterized by significant advancements in building techniques. Over time, the architecture of the Song Dynasty accumulated a wealth of climate-responsive design measures, while only a few buildings from this time have been retained^{7,8}. Fortunately, the paintings of the Song Dynasty, renowned for their realism and meticulous details, contain rich information on building components and structures (a.k.a. the way of assembling building components)⁹. This study investigates the architectural component “Yinyan”, as depicted in the paintings of the Song Dynasty,

focusing on its impact on indoor wind environments. It aims to extract the design wisdom embedded in traditional architecture. The findings are expected to enrich the multi-sensory digital representation of architectural heritage in the Song Dynasty and offer insights for both the conservation of Song architectural heritage and the sustainable design of contemporary architecture.

The digitalization of architectural heritage is undergoing diversified development, with accurate and efficient 3D representation widely regarded as its fundamental core. Zhou et al. integrated multi-source historical images and employed shape grammar analysis in combination with parametric design algorithms, significantly improving the efficiency of modeling Song Dynasty architecture¹⁰. To address the challenge of replicating repetitive textures and structural patterns in historic buildings, Yao et al. proposed a self-attention-guided unsupervised single image-based depth estimation method, offering a novel approach to high-precision 3D representation¹¹. Valenti et al. conducted a comprehensive digital reconstruction of the Saint Lucia di Mendola site by combining archive research, geometric analysis, high-resolution 3D scanning and photogrammetry, digital recomposition of architectural fragments, and virtual modeling techniques¹². The application of digital technologies in architectural heritage has expanded beyond traditional documentation and conservation. It now encompasses risk

¹Huzhou University, Art School, Huzhou, China. ²Xi'an Jiaotong-Liverpool University, Design School, Suzhou, China. ³Xi'an University of Architecture and Technology, School of Architecture, Xi'an, China. ✉e-mail: x_purple@foxmail.com; bing.chen@xjtlu.edu.cn

detection and mitigation, facility management, immersive educational experiences, and public engagement^{13,14}. For example, De Fino et al. introduced a 360° thematic virtual tour system that integrates various digital resources to support cultural dissemination, performance evaluation, and risk management of historic buildings¹⁵. Nguyen et al., using the Temple of Hung Kings in Vietnam as a case study, applied Scan-to-HBIM technologies for digital reconstruction and incorporated tools such as VR and AR for building management and tourism promotion¹⁶. Milic et al., through a real-world architectural heritage project, explored new pedagogical strategies for architectural history education, integrating field surveys, data processing, and BIM model development¹⁷. Among these, the educational value of digital heritage is increasingly recognized as a key dimension that transcends technological innovation. As a bridge between heritage and societal value, the accurate digital representation of architectural heritage holds significant potential for revealing cultural meaning and enhancing educational impact. This is an area that deserves further exploration.

Traditional architecture around the world has gradually developed climate-adaptive features in response to local environmental conditions^{18–20}. Among various passive design strategies, natural ventilation has been widely researched due to its effectiveness in enhancing indoor comfort. Previous studies have explored not only the influence of spatial layout and architectural form in traditional villages on airflow patterns, but also the role of specific building components in regulating indoor ventilation^{21–23}. For example, Aydin and Mirzaei examined the function of “Cumba” in traditional Turkish architecture and found that it could significantly improve indoor ventilation. When combining it with flexible window-opening strategies, both the average wind speed and ventilation rate could be adjusted towards a wide range²⁴. Similarly, Suleiman and Himmo analyzed the “Malqaf” in Arab traditional architecture and explored its ability to channel wind into buildings to create a comfortable wind environment²⁵. Climate-adaptive building components can be flexibly adjusted to respond to varying climatic conditions. However, limited attention has been paid to such components of traditional Chinese architecture.

To summarize, substantial progress has been achieved in the digital representation of architectural heritage, particularly in 3D modeling technologies, information management, and practical applications, which have strongly supported heritage conservation and dissemination. In the field of natural ventilation and climate-responsive design, previous research has examined how various design strategies, such as building layouts, spatial organization, and building components, affect indoor wind environments, thereby confirming the value of traditional climate-adaptive design strategies. However, in-depth studies focusing specifically on the climate adaptability of Song Dynasty architecture remain limited. Moreover, research on multi-sensory digital representation of architectural heritage seldom explores the relationship between climate-adaptive building components and human indoor perception, which constrains the effective transmission of design wisdom embedded in traditional architecture. This study looks into Chinese traditional architecture from the Song Dynasty. By integrating historical paintings, literature, and preserved architectural heritages, we build the digital mock-up of buildings from the Song Dynasty and employ numerical simulations to assess the impact of the building component “Yinyan” on indoor ventilation. It aims to provide scientific evidence for the accurate digital representation of “Yinyan” and provide insights for both the conservation and restoration of Song architectural heritage, as well as the climate-responsive design of contemporary architecture.

Methods

The overall research design is shown in Fig. 1. Based on paintings and historical archives from the Song Dynasty, a digital model of a traditional building from the Song Dynasty was constructed. The Computational Fluid Dynamics (CFD) numerical simulations were then conducted to investigate the impact of the building component “Yinyan” on the indoor wind environment.

The digital mock-up of traditional architecture based on Song Dynasty paintings

Research on the digital representation of architectural heritage based on iconographic evidence has gained increasing attention in recent years^{10,26}. “Wumu” painting, one of the ten prevailing painting genres of Song Dynasty in China, employed scientific tools such as scale bars to illustrate cityscapes, buildings, and their surrounding natural environments with exceptionally high precision. Artists were required to maintain precise proportions and details in paintings, making the paintings function equally to modern architectural blueprints²⁷. Chiu et al. rebuilt the scenes portrayed in *Life along the Bian River at the Qing Ming Festival* (*Qing Ming Shang He Tu* in Pinyin), a famous painting by Zhang Zeduan of the Northern Song Dynasty, and analyzed the seasonal context depicted in the painting^{28,29}. Dong utilized the wooden pavilions from paintings of the Song Dynasty as a reference, along with *Yingzao Fashi*, an official building construction guide in the Song Dynasty, to rebuild the mock-up pavilions of the Song Dynasty^{30,31}. These studies demonstrate that, by integrating “Wumu” paintings with historical archives and preserved architectural heritages from the Song Dynasty, it is feasible to replicate the traditional buildings in the Song Dynasty as well as their architectural components.

Architectural component “Yinyan” in Song Dynasty paintings

During the Northern Song Dynasty, Bianjing (current Kaifeng City located in Henan Province) experienced low rainfall and frequent sandstorms³². To cope with these climatic conditions, a transitional space has often been added between indoor and outdoor spaces. The “Yinyan”, a typical climate-responsive building component, was widely adopted for this purpose due to its ease of installation and replacement³³. It typically consisted of a wooden frame inlaid with wooden panels or bamboo strips and was affixed to exterior walls. This component was frequently noted in the paintings of Song Dynasty, including *Life along the Bian River at the Qing Ming Festival* by Zhang Zeduan, *Reading the Book of Change in a Cottage* (*Qiu Chuang Du Yi Tu* in Pinyin) by Liu Songnian, and other notable works such as *Nine Elders Enjoying a Gathering in the Huichang Period* (*Hui Chang Jiu Lao Tu* in Pinyin), *Autumn Trees and Mountains* (*Qiu Shan Hong Shu Tu* in Pinyin), *Conversation in Snowy Hall* (*Xue Tang Ke Hua Tu* in Pinyin) and *Boating on a Lotus Pond* (*Lian Tang Fan Ting Tu* in Pinyin) (Fig. 2)^{29,34}.

Based on the analysis of these paintings, it was found that “Yinyan” was typically installed by attaching one long edge to the eaves or the upper frame of a window located beneath the eaves. The opposite long edge was either left unsupported (Fig. 2a, d)) or reinforced with diagonal braces (Fig. 2b, e, f).

Architectural components depicted in the painting of “Life along the Bian River at the Qing Ming Festival” and the mock-up building designs

This research selects a two-story tavern, with two standard rooms, located next to the Rainbow Bridge in the *Life along the Bian River at the Qing Ming Festival* (Fig. 2a), for further study. Using the digital mock-up of this building, this research investigates the impacts of the position and lengths of “Yinyan” on the indoor wind environment of traditional buildings in the Song Dynasty.

“Zhang”, “chi”, and “cun” are traditional Chinese length units, where 1 “zhang” is equal to 10 “chi”, and 1 “chi” is equal to 10 “cun”. During the Song Dynasty, the length of 1 “chi” was not unified across regions. In the book *History of Ancient Chinese Architecture*, Liu reported that the length of 1 chi ranged from 0.309 to 0.329 meters across different regions³⁵. This study adopts a standardized mean value of 0.32 m for 1 chi, corresponding to 3.2 m for 1 zhang and 0.032 m for 1 cun.

“Wumu” paintings employed a drawing method similar to modern oblique axonometric projections³⁶. In the selected painting, parallel lines were drawn along the ridge, eaves, and railings of the tavern’s main facade (Fig. 3). Since the extensions of these lines do not intersect, it can be inferred that the facade is depicted in a nearly parallel projection. Measurements of the height of columns and the width of rooms in the painting reveal a column height-to-room width

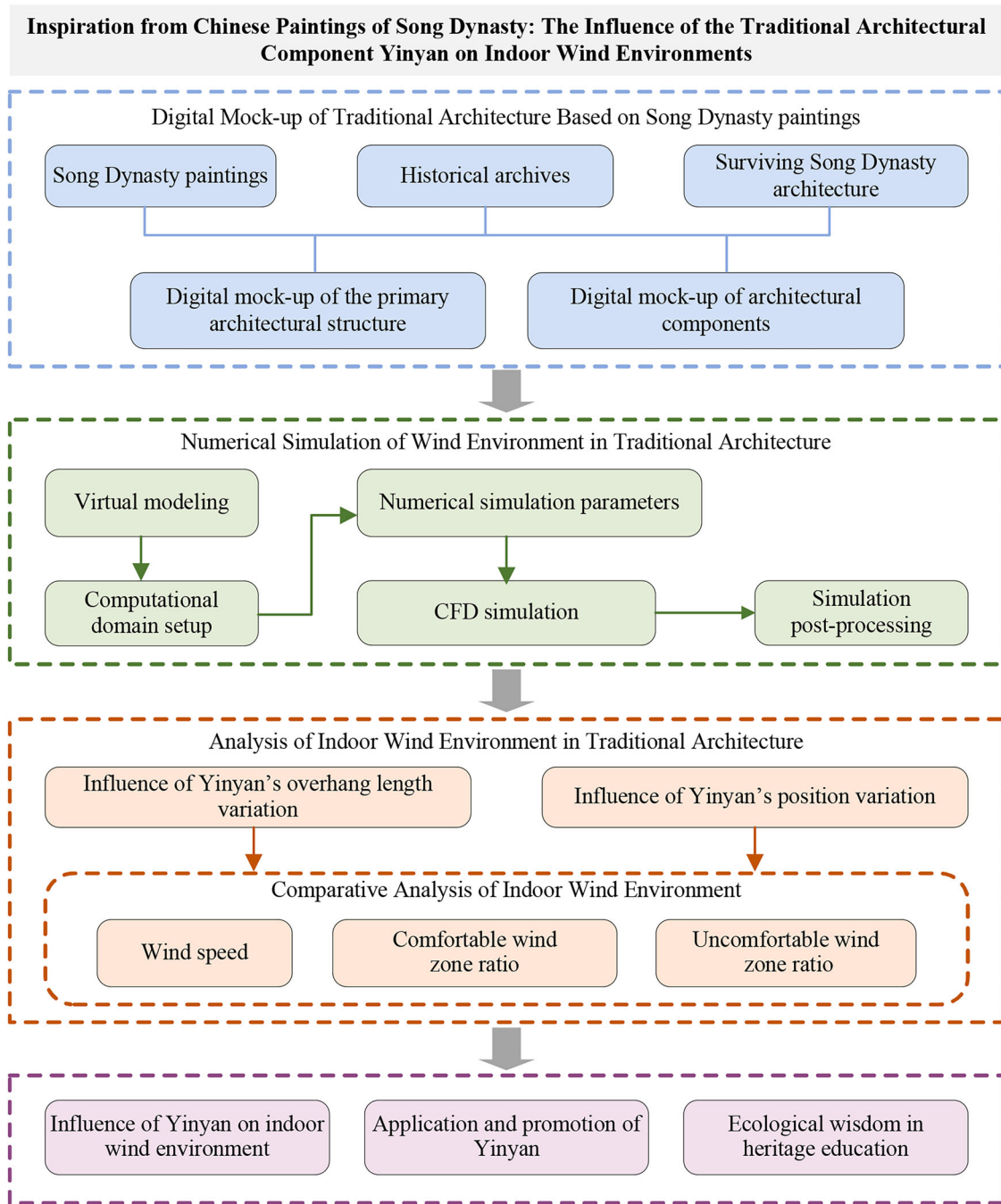


Fig. 1 | Flowchart of the research process adopted in this study.

ratio of approximately 0.72 (Fig. 3). Wang’s survey and analysis of architectural heritages from the Tang and Song Dynasties (e.g., the Main Hall of Baoguo Temple, the Shanmen of Dule Temple, and the Xiandian of Jinci Temple) found that, in small-scale Tang and Song buildings (2–3 standard rooms), the column height-to-room width ratio typically ranged from 0.70 to 0.74³⁷. Since the ratio of 0.72 derived from the painting fits into this range, it becomes reasonable to build the digital mock-ups of Song buildings referring to the “Wumu” paintings.

Historical records and preserved buildings from the Song Dynasty indicate that the width of a standard room was normally in a range of 1.8–1.2 zhang (e.g., 1.8 zhang, 1.5 zhang, 1.3 zhang, or 1.2 zhang)³⁰. Assuming the room width of this tavern is 1.3 zhang (equal to 4.16 m) and applying the column height-to-room width ratio of

0.72, the estimated column height is 2.88 m. For small-scale buildings in the Song Dynasty, the roof height (a.k.a. the vertical distance between the ridge of the roof and the eaves) is typically approximately two-thirds of the column height, so the estimated roof height is 1.92 m³⁷. Additionally, based on this scale, the measured height of a seated figure in the painting is approximately 1.26 m (Fig. 3), which aligns with the typical height of a seated person. This further validates the inferred room width. Based on the surveying results of preserved buildings from the Song Dynasty and the relevant studies, the width-to-depth ratio of a single-span structure is approximately 1:1³⁷, indicating that the depth of the tavern is also 4.16 m. Further referring to *Yingzao Fashi*, the first-floor height and other structural details were speculated, forming the mock-up of the tavern³⁸. Fig. 4 presents the digital mock-up of the building with key components.

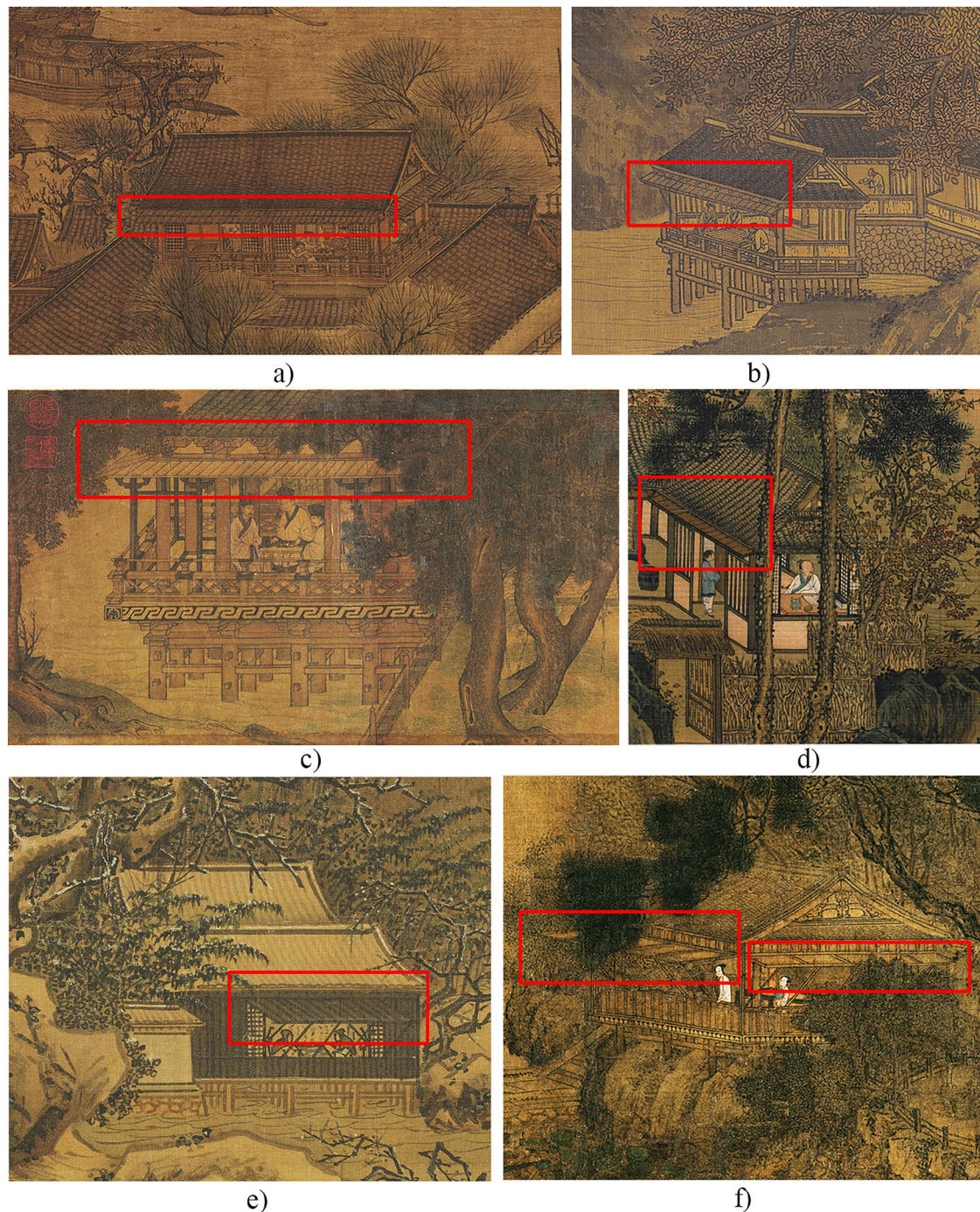


Fig. 2 | Yinyan in partial views of Song Dynasty paintings. **a** *Life along the Bian River at the Qing Ming Festival*; **b** *Autumn Trees and Mountains*; **c** *Nine Elders Enjoying a Gathering in the Huichang Period*; **d** *Reading the Book of Change in a Cottage*; **e** *Conversation in Snowy Hall*; **f** *Boating on a Lotus Pond*.

Virtual modeling for numerical simulation

Based on paintings of the Song Dynasty, “Yinyan” could be installed either at the eaves or in between the window frames and the eaves, with variations in size. Preliminary CFD simulations indicated that variations in the angle of the “Yinyan” had a rather limited impact on indoor ventilation. Therefore, this study focuses on the influence of Yinyan’s overhang length and position on indoor wind environments. In the digital model, the overhang length is estimated at approximately 0.96 m based on proportional analysis of the painting. According to the *Yingzao Fashi*, the overhang length of Yinyan ranged from 3 to 5 chi (equal to 0.96–1.6 m)³⁸. Given that the depth of the traditional building in this study is relatively small (4.16 m), four overhang

lengths of the “Yinyan” were selected for comparative studies: 3 chi (equal to 0.96 m), 3.5 chi (1.12 m), 4 chi (1.28 m), and 4.5 chi (1.44 m). As summarized in Table 1, the impact of “Yinyan” on indoor ventilation was analyzed across eight scenarios, taking into account two installation positions and four overhang length settings. Case 1 represents the mock-up based on the painting and will be used for preliminary numerical simulation and model calibration.

To facilitate numerical simulations and comparative analyses, the tavern was simplified in the digital model, with building components such as windows and “Yinyan” being replaced by flat panels. The simplified model for Case 1 is illustrated in Fig. 5.

Fig. 3 | Tavern's main facade and inferred room width, column height, and roof height.

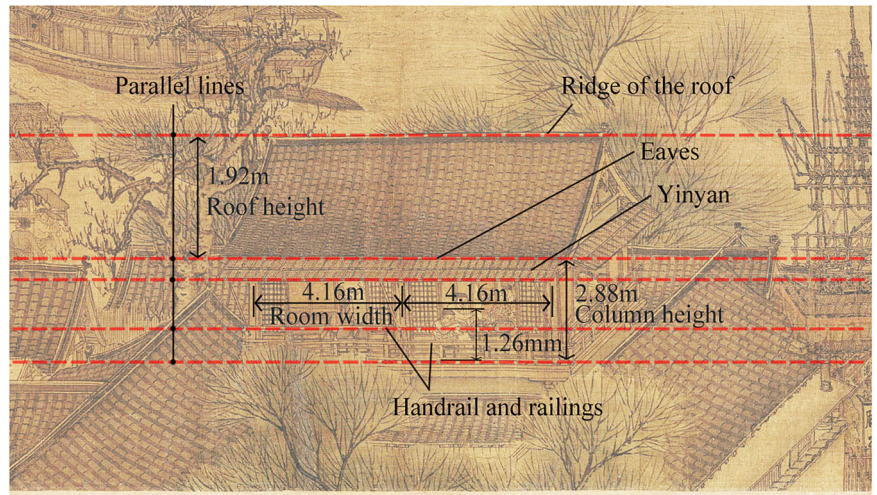
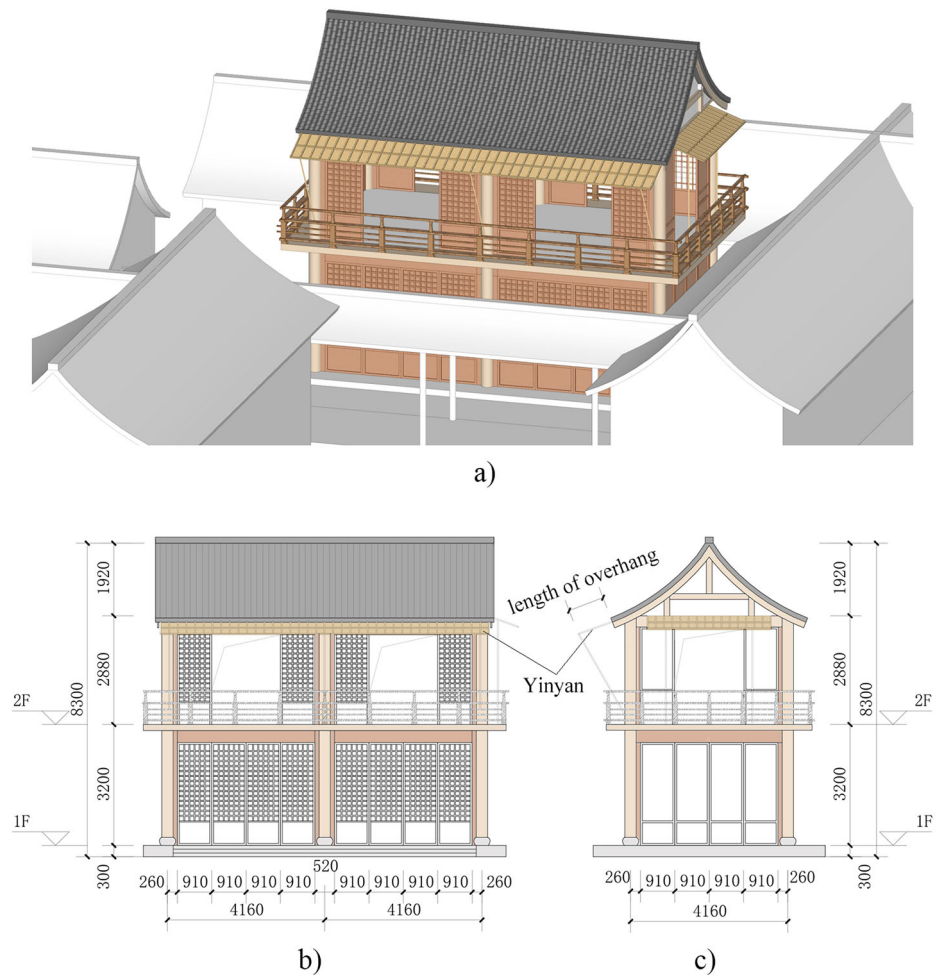


Fig. 4 | Mock-up design of the tavern. **a** 3D model; **b** Front elevation; **c** Side elevation (unit: mm).



Parameter settings for numerical simulation

In terms of the computational domain, the building footprint occupies less than 3% of the total computational domain. The target building was positioned at a distance of 3H (where H represents the maximum height of the target building) from the inlet boundary, 5H from the side boundaries, 10H from the outlet boundary, and 5H from the top boundary³⁹. In this numerical simulation, the maximum height of the target building was

approximately 8.3 meters. In return, the distances to the inlet boundary, outlet boundary, side boundaries, and top boundary were set to 24.9 m, 83 m, 41.5 m, and 41.5 m, respectively (Fig. 6).

In this study, a polyhedral unstructured mesh was employed for simulation. First, a base mesh size was defined for the computational domain, with finer meshes applied to the building and its surrounding areas, and even finer meshes assigned to building components to ensure that each

complete boundary of the building contained at least 10 meshes. Additionally, boundary layer meshes were generated on the ground surface. A mesh sensitivity analysis was conducted (see Section Mesh Sensitivity Analysis). Based on the results, the base mesh size was set to 4 m. The relative mesh sizes for the building components and surrounding ground are summarized in Table 2. To improve the simulation accuracy, the mesh within the second-floor interior of the tavern was further refined, with a refined mesh size set to 3% of the base mesh size. The volumetric growth rate

between adjacent mesh cells was set to 1.2. The mesh configuration for Case 1 is illustrated in Fig. 7, with approximately 1.06 million meshes generated for the entire computational domain.

For the physical model, the computational domain was modeled as a space full of steady-state, constant-density gas. The Realizable $k-\epsilon$ model was chosen for the simulation. The accuracy of this model in simulating wind environments around clustered buildings has been validated in previous studies, with an identified error within an acceptable range⁴⁰⁻⁴².

The inlet boundary was defined as a velocity inlet, and the turbulence model was set to the Realizable $k-\epsilon$ model. Chiu et al. compiled wind speed data of Kaifeng City from the past 50 years to simulate the scenario illustrated in *Life along the Bian River at the Qing Ming Festival*, and found that prevailing winds blew from the south to the north in spring and from the northeast to the southwest in autumn, with an average wind speed of approximately 3.0 m/s³⁸. In Kaifeng, natural ventilation was often used during spring and early summer to provide better indoor air quality and thermal comfort. Therefore, this study adopts a south wind direction with a wind speed of 3.0 m/s for the simulation. The vertical velocity profile $U(z)$,

Table 1 | Summary of Yinyan case study scenarios used in numerical simulation

Installation Position	Overhang length			
	3 chi 0.96 m	3.5 chi 1.12 m	4 chi 1.28 m	4.5 chi 1.44 m
Installed at the eaves	Case1	Case2	Case3	Case4
Installed above the window frame	Case5	Case6	Case7	Case8

Fig. 5 | Simplified model.

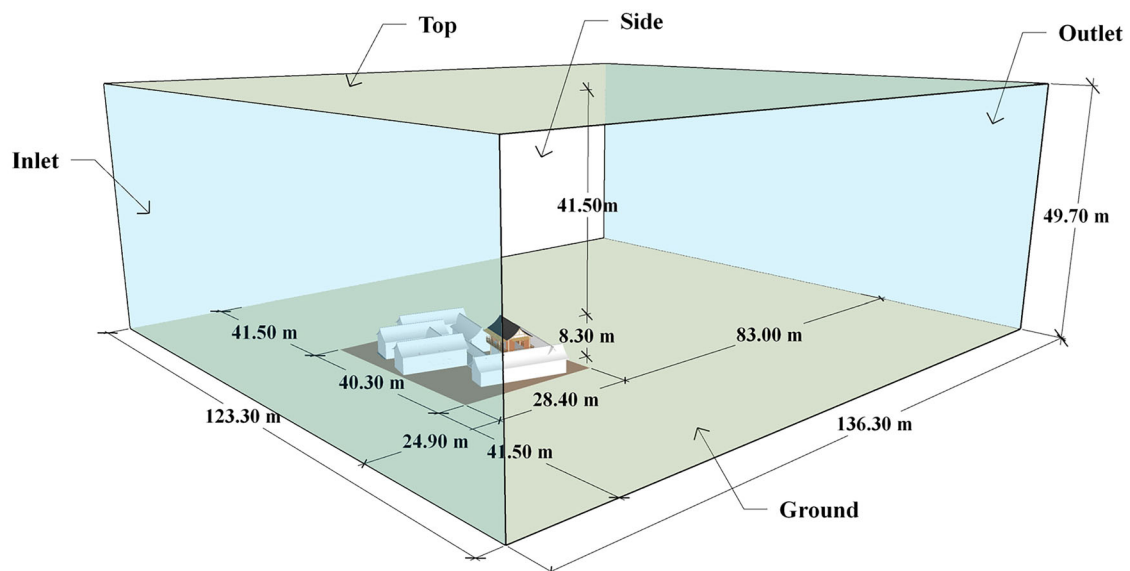
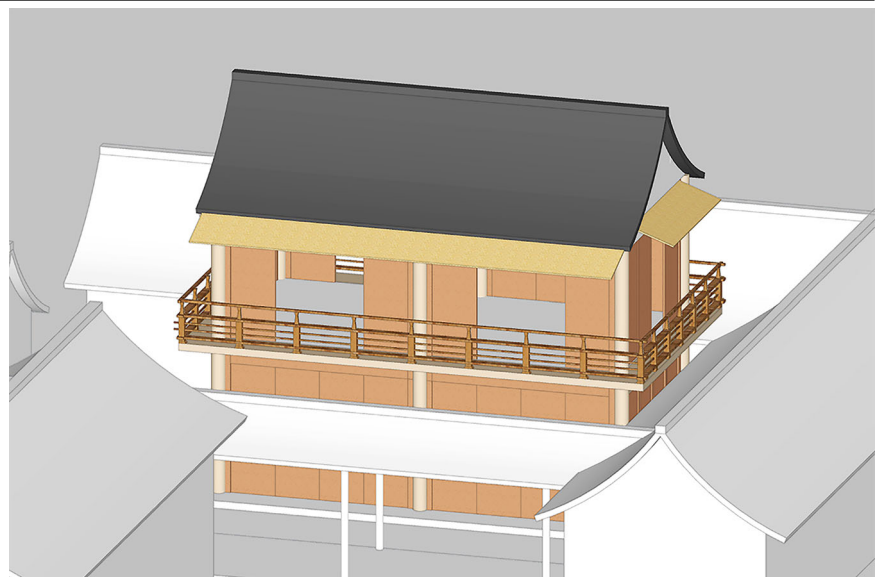


Fig. 6 | Computational domain and position of the traditional building.

turbulent kinetic energy (k), and turbulent energy dissipation rate (ϵ) were calculated by Eqs. (1)–(4)^{39,43}.

$$U(z) = U_s \left(\frac{z}{z_s} \right)^\alpha \tag{1}$$

$$I(z) = \frac{\sigma_u(z)}{U(z)} = 0.1 \left(\frac{z}{z_G} \right)^{(-\alpha-0.05)} \tag{2}$$

$$k(z) = \frac{\sigma_u^2(z) + \sigma_v^2(z) + \sigma_w^2(z)}{2} \cong \sigma_u^2(z) = (I(z) * U(z))^2 \tag{3}$$

$$\epsilon(z) \cong C_\mu^{1/2} k(z) \frac{U_s}{z_s} \alpha \left(\frac{z}{z_s} \right)^{\alpha-1} \tag{4}$$

In these equations, U_s is the wind speed at the reference height, set to 3.0 m/s, and z_s is the reference height, set at 10 meters. z is the actual height, and $U(z)$ is the wind speed at height z . The surface roughness index α is set to 0.15⁴⁴. $\sigma_u(z)$ is the root mean square value of the velocity in the flow direction. The boundary layer height z_G , corresponding to the terrain category, is set to 350 m. C_μ is a constant, with a value of 0.09.

The outlet boundary was defined as a pressure outlet, with the initial values of pressure, turbulent kinetic energy, and turbulent dissipation rate all

set to 0. All other parameters were kept at their default settings in the numerical simulations.

The side and top boundaries, as well as the building surfaces, were defined as smooth walls.

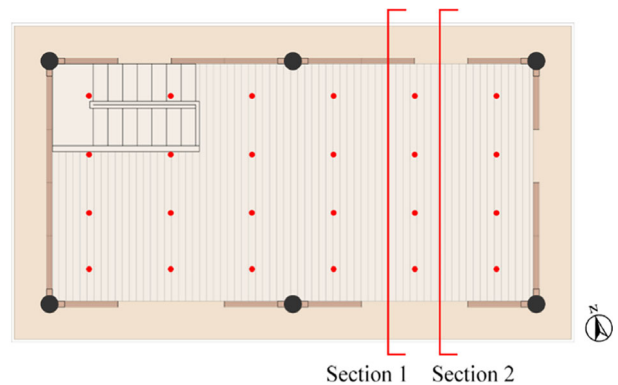
The ground boundary was defined as a rough surface, with a roughness height set to 1.8×10^{-4} m.

Indoor wind environment evaluation

The second floor of the tavern was designated as the evaluation area. Two sections, Section 1 and Section 2, as shown in Fig. 8, were defined within this area to analyze the vertical distribution of indoor airflow under Case 1, Case 5, and the scenario without the “Yinyan” installed. Following the studies of Yang & Zhang, based on evaluation methods for indoor environments outlined in ASHRAE Standard 55 and GB-50785⁴⁵⁻⁴⁷, two horizontal evaluation planes were defined: one at 1.1 m above the 2nd floor, representing

Table 2 | Relative mesh sizes for the architectural components and the surrounding ground

Region and component	Mesh size/base mesh size
Buildings and the surrounding ground area	10%
Walls	3%
Roofs	3%
Windows	3%
Handrail and railings	1%
Yinyan	1%



● Test point

Fig. 8 | The 2nd floor plan of the tavern, the locations of two sections, and the 24 test points.

Fig. 7 | Mesh configuration for Case 1. a Mesh within the computational domain; b Mesh near the building.

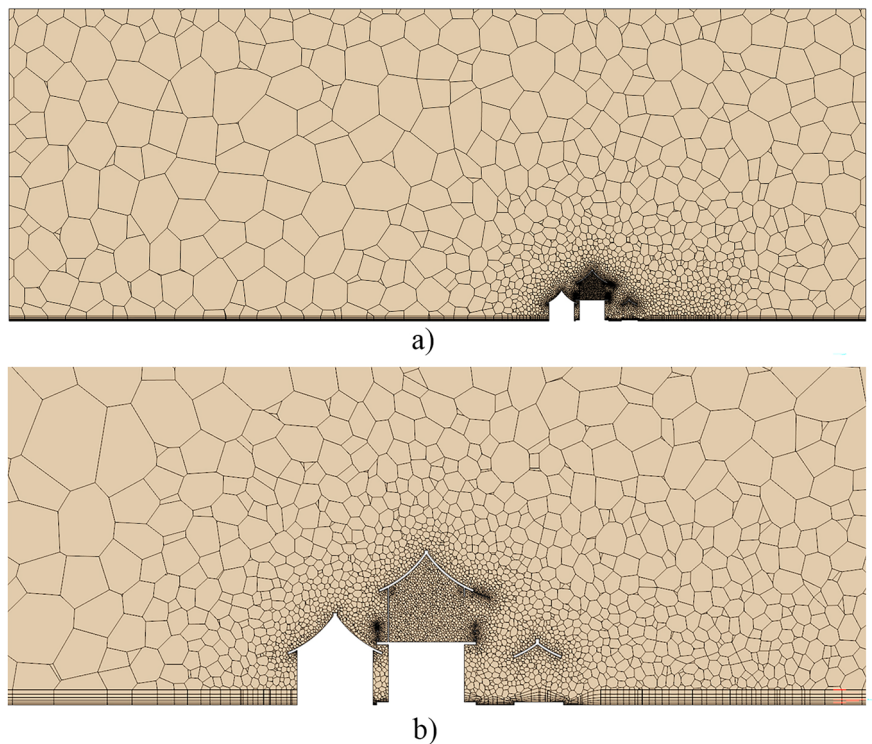


Fig. 9 | Wind speed values at the 24 test points under four base mesh sizes.

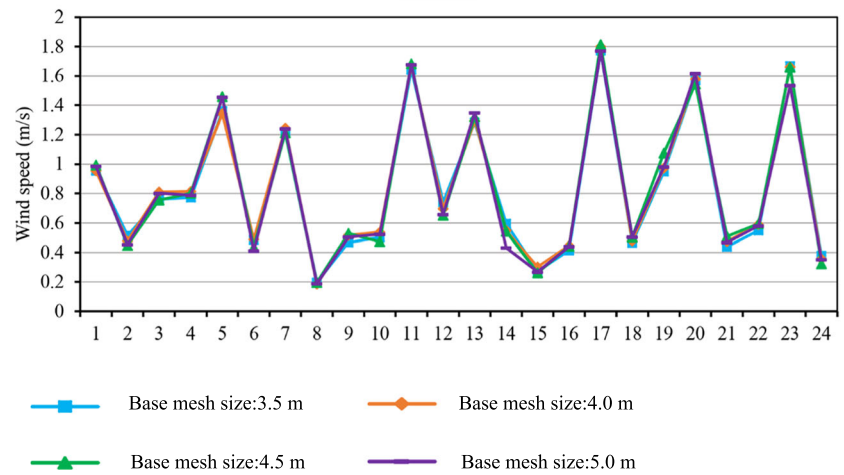
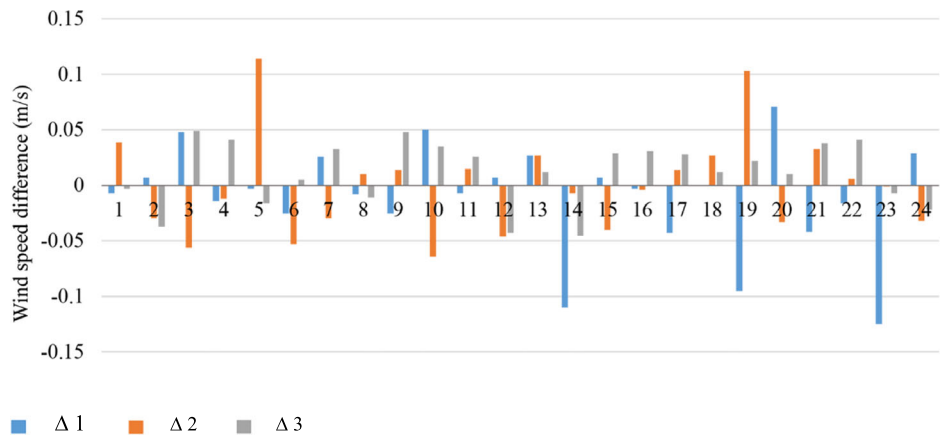


Fig. 10 | Comparison of wind speed differences at the 24 test points under different mesh configurations.



head and shoulder height when seated, and another at 1.7 m, representing head and shoulder height when standing.

In naturally ventilated indoor environments, wind speed has a critical impact on human thermal comfort⁴⁸⁻⁵¹. Previous studies indicated that most individuals perceived wind speeds ranging from 0.25 to 1.0 m/s as comfortable. In warmer climatic conditions, some occupants might tolerate wind speeds between 1.0 and 1.5 m/s. However, wind speeds exceeding 1.5 m/s would often cause discomfort as the wind might shift lightweight indoor objects, while speeds below 0.25 m/s would hinder the effect of removing indoor air pollutants^{52,53}.

For this study, the indoor wind environment was categorized into three zones: the comfortable wind zone (wind speed: 0.25–1.0 m/s), the stagnant wind zone (wind speed <0.25 m/s), and the excessive wind zone (wind speed >1.5 m/s). Wind speeds between 1.0 and 1.5 m/s would result in varied subjective responses - some individuals perceive them as uncomfortable, while others consider them acceptable⁵³. Therefore, this range is excluded from the present analysis. To facilitate the comparative studies, the stagnant and excessive wind zones were collectively defined as uncomfortable wind zones. Computational modules were developed within the simulation software to explore the comfortable wind zone ratio (i.e., the proportion of the evaluation area within the comfortable range) and the uncomfortable wind zone ratio (i.e., the proportion of the evaluation area within the uncomfortable range). These modules were used to evaluate the effects of Yinyan on the indoor wind environments according to its different lengths and locations.

Mesh sensitivity analysis

According to the computational settings outlined in Section Parameter Settings for Numerical Simulation, a mesh sensitivity analysis was

conducted for Case 1 using different base mesh sizes. The base mesh sizes were set to 5 m, 4.5 m, 4 m, and 3.5 m. The relative mesh sizes for the building components and surrounding ground are summarized in Table 2. To evaluate the impact of mesh sizes on wind speed predictions, 24 test points were selected at a height of 1.1 m above the 2nd floor of the tavern (Fig. 8). Figure 9 presents the comparison of wind speed values at the 24 test points under the four mesh sizes. The overall wind speed trends remain consistent across all conditions. However, under the 5 m mesh configuration, some test points exhibited slightly higher deviations. To further analyze the simulated wind speed differences at the 24 test points under different mesh configurations, the differences were calculated between the 5 m and 4.5 m meshes (denoted as Δ1), the 4.5 m and 4 m meshes (denoted as Δ2), and the 4 m and 3.5 m meshes (denoted as Δ3). A comparison of these differences is shown in Fig. 10. The values of Δ1 and Δ2 are relatively larger, while Δ3 is smaller and remains below 0.05 m/s. This indicates that the wind speed predictions at the 24 test points are relatively consistent when the mesh configurations fall into 3.5–4 m, with no significant discrepancies. Considering that the 3.5 m mesh would require higher computational costs, the 4 m mesh was ultimately selected as the base mesh for the numerical simulations in this study.

Results

Influence of Yinyan on the vertical distribution of indoor airflow

Figure 11 illustrates the vertical airflow distributions for Case 1, Case 5, and the scenario without the “Yinyan”. Section 1 represents a vertical plane with a single-sided opening. Without “Yinyan” (Fig. 11a), the incoming airflow enters at a downward angle and gradually loses velocity. Upon reaching the rear wall, it rises, forming a stagnant zone near the rear wall and a relatively large vortex in the upper rear region. In Case 1 (Fig. 11b), where the

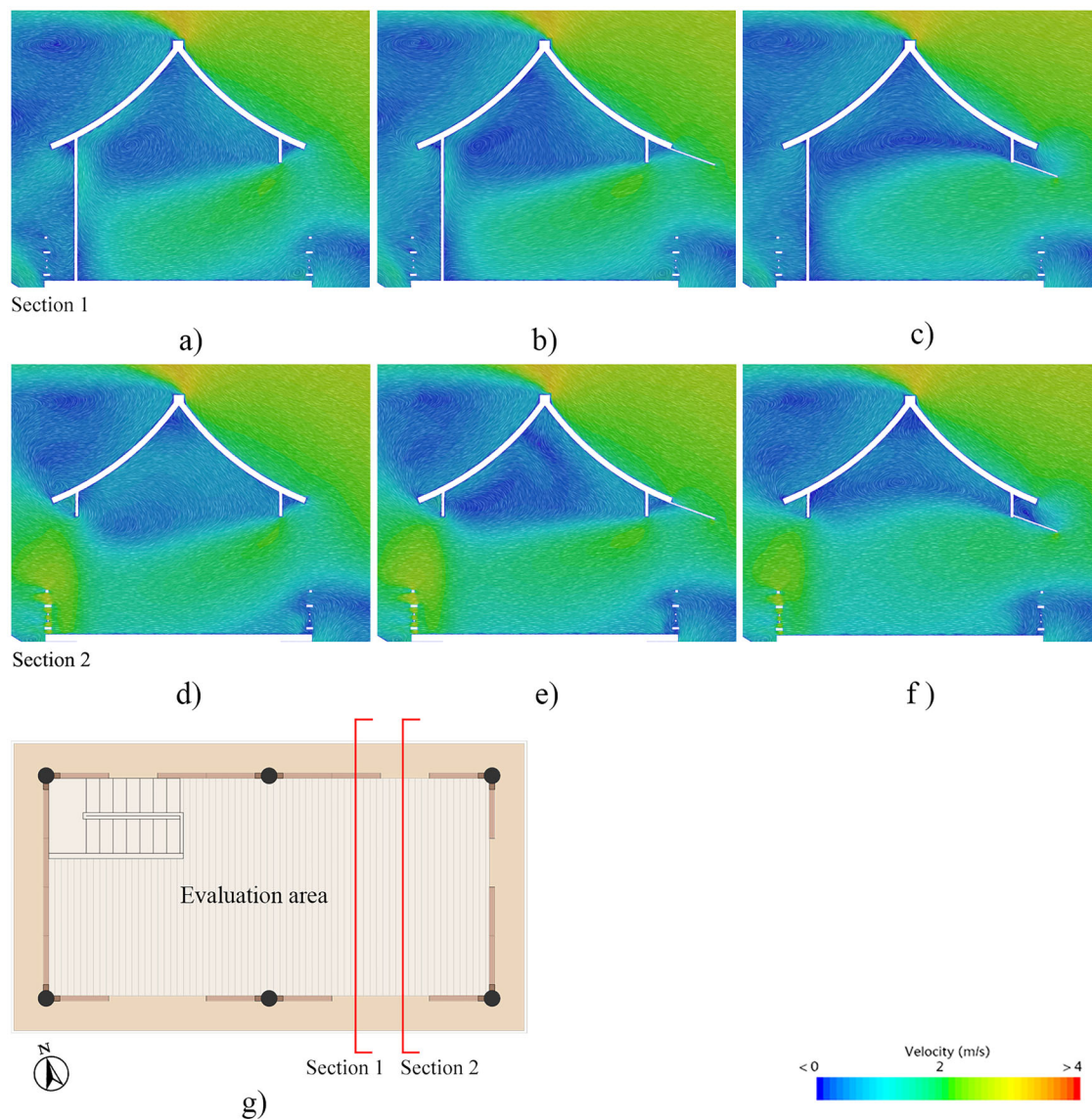


Fig. 11 | Vertical airflow distributions. a Scenario without the “Yinyan”, Section 1; b Case 1, Section 1; c Case 5, Section 1; d Scenario without the “Yinyan”, Section 2; e Case 1, Section 2; f Case 5, Section 2; g Locations of Sections 1 and 2.

“Yinyan” is installed at the eaves, the airflow follows a similar downward path but with slower velocity attenuation due to the guiding effect of the “Yinyan”. And the upper vortex shifts closer to the rear wall. In Case 5 (Fig. 11c), where the “Yinyan” is installed above the window frame, the airflow diffuses more broadly into the room, reducing the stagnant zone and shifting the upper vortex towards the central upper area, where it becomes smaller in size.

Section 2 represents a vertical plane with openings on both sides, enabling cross-ventilation. Without the “Yinyan” (Fig. 11d)), the airflow enters at a downward angle with gradually decreasing velocity, then inclines upward near the rear of the room before exiting. A relatively large vortex forms in the upper rear region. In Case 1 (Fig. 11e)), with the “Yinyan” installed at the eaves, the airflow travels more horizontally across the room, resulting in smoother and more uniform flow. The upper vortex shifts towards the rear corner. In Case 5 (Fig. 11f)), with the “Yinyan” installed above the window frame, the guiding effect causes the incoming airflow to diffuse slightly, expanding the affected area. The upper vortex moves towards the central upper region and becomes more dispersed.

Overall, the “Yinyan” exerts a significant impact on indoor airflow. When installed at the eaves, it increases airflow penetration and average

indoor wind speed, thereby improving the indoor wind environment. When installed above the window frame, it alters airflow direction, promotes diffusion, and expands the effective flow area.

Influence of Yinyan’s overhang length on the indoor wind environment when installed at the eaves

When the “Yinyan” was installed at the eaves, the indoor wind speed contour plots for Cases 1 to 4 are shown in Fig. 12. The results indicate that the overall indoor airflow patterns are consistent across all cases. Higher wind speed areas are primarily located along the airflow paths aligned with the two door-window openings, while lower wind speed stagnant zones are situated between these airflow paths.

As the Yinyan’s overhang length increases, the stagnant wind zone area on the 1.1 m evaluation plane remains relatively unchanged (Fig. 12). However, the area of the comfortable wind zone (especially those with wind speed: 0.25–0.5 m/s) gradually expands, while the uncomfortable wind zone (especially those with wind speed >1.75 m/s) progressively shrinks and eventually disappears. On the 1.7 m evaluation plane, the increase of Yinyan’s overhang length leads to a gradual decrease in the uncomfortable wind zone (especially those with wind

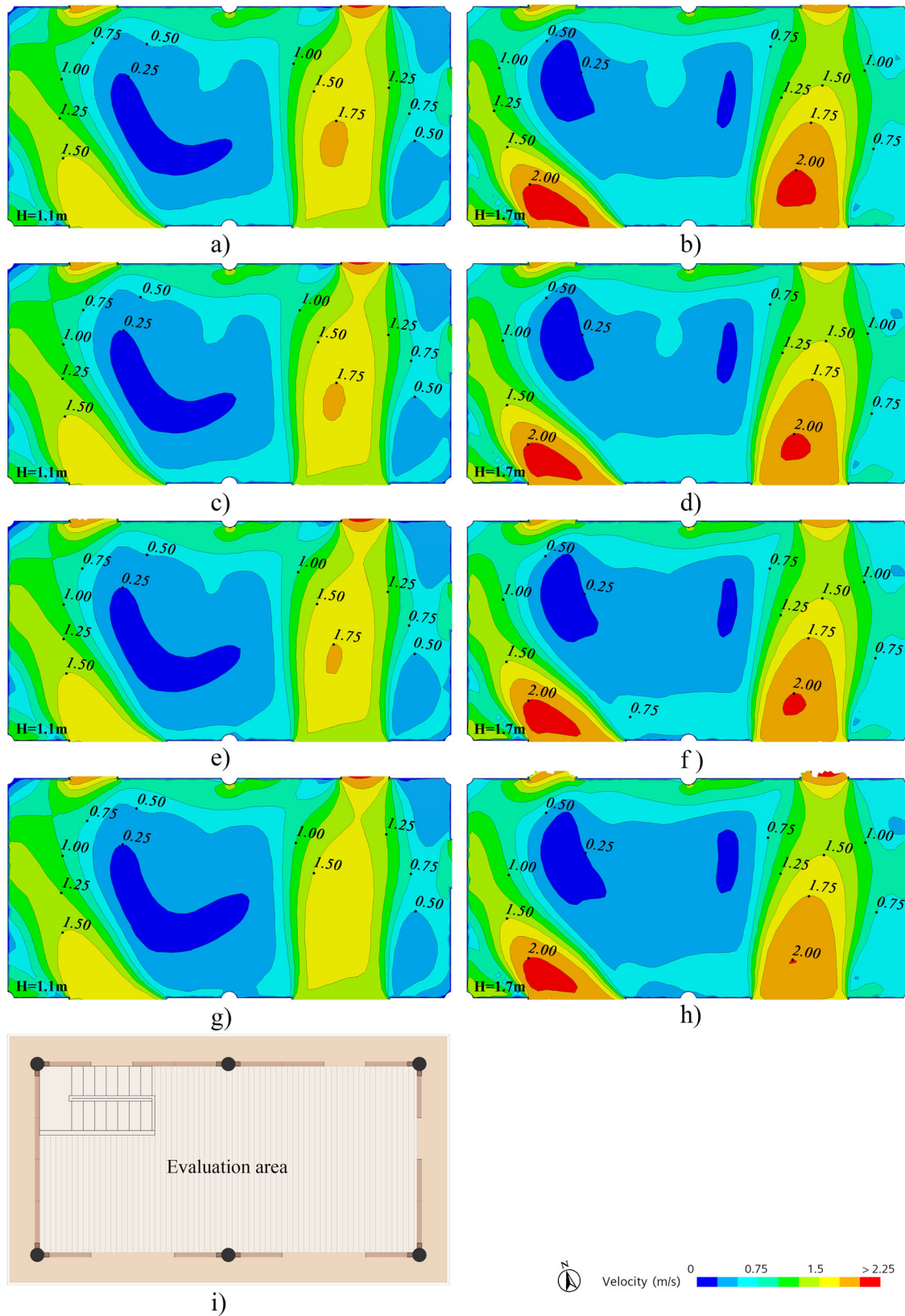


Fig. 12 | Indoor wind speed contour plots under different scenarios. a Case 1, 1.1 m evaluation plane; b Case 1, 1.7 m evaluation plane; c Case 2, 1.1 m evaluation plane; d Case 2, 1.7 m evaluation plane; e Case 3, 1.1 m evaluation plane; f Case 3,

1.7 m evaluation plane; g Case 4, 1.1 m evaluation plane; h Case 4, 1.7 m evaluation plane; i The 2nd floor plan of the tavern.

Table 3 | Indoor wind conditions with Yinyan installed at the eaves

	1.1 m evaluation plane					1.7 m evaluation plane				
	Wind speed (m/s)			Wind zone ratios		Wind speed (m/s)			Wind zone ratios	
	Max	Min	Avg.	Comfortable	Uncomfortable	Max	Min	Avg.	Comfortable	Uncomfortable
Case 1	2.33	0.030	0.89	55.74%	21.82%	2.24	0.031	0.92	59.36%	21.75%
Case 2	2.32	0.026	0.88	55.95%	21.63%	2.23	0.039	0.92	59.31%	22.03%
Case 3	2.34	0.018	0.88	55.93%	21.41%	2.24	0.046	0.91	59.10%	22.44%
Case 4	2.34	0.026	0.86	55.59%	21.65%	2.23	0.053	0.90	58.63%	22.93%

speed >2 m/s) and a significant increase of the comfortable wind zone (especially those with wind speed: 0.25–0.5 m/s).

The simulated indoor wind environment for Cases 1–4 are summarized in Table 3. As the Yinyan’s overhang length varied, the maximum wind speed on the 1.1 m evaluation plane ranged from 2.32 to 2.34 m/s, while the minimum wind speed ranged from 0.018 to 0.030 m/s. On the 1.7 m evaluation plane, the maximum wind speed ranged from 2.23 to 2.24 m/s, and the minimum wind speed ranged from 0.031 to 0.053 m/s. The relatively small variations in both maximum and minimum wind speeds indicate a weak correlation between Yinyan’s overhang length and indoor wind speeds.

The average wind speed on the 1.1 m evaluation plane ranged from 0.86 to 0.89 m/s, while on the 1.7 m evaluation plane, it ranged from 0.90 to 0.92 m/s. With the increase of Yinyan’s overhang length, the indoor average wind speed showed a slightly decreasing trend, though the difference was small.

Changes in Yinyan’s overhang length had little impact on the comfortable and uncomfortable wind zone ratios on the 1.1 m evaluation plane. On the 1.7 m evaluation plane, slight variations were observed: the comfortable wind zone ratio gradually decreased, while the uncomfortable wind zone ratio increased.

To summarize, when the “Yinyan” is installed at the eaves, variations in its overhang length have a limited impact on the maximum and minimum indoor wind speeds. However, the average indoor wind speed gradually decreases as Yinyan’s overhang length increases. On the 1.7 m evaluation plane, the comfortable wind zone ratio gradually decreases, while the uncomfortable wind zone ratio increases, though the changes remain relatively small. The worst conditions are observed in Case 4, where Yinyan’s overhang length is 1.44 m.

Influence of Yinyan’s overhang length on the indoor wind environment when installed above the window frame

The indoor wind speed contour plots for Cases 5 to 8 are shown in Fig. 13, illustrating that the overall indoor airflow patterns remain consistent across all cases. Higher wind speed areas are primarily located along the airflow paths aligned with the door-window openings, while stagnant zones with lower wind speeds are situated between these airflow paths.

On the 1.1 m evaluation plane, the stagnant wind zone is mainly distributed on the southern side between the two airflow paths. As the Yinyan’s overhang length increases, the stagnant zone initially decreases and then increases. The excessive wind zone shrinks with increased Yinyan’s overhang length. On the 1.7 m evaluation plane, as the Yinyan’s overhang length increases, the stagnant wind zone remains relatively stable, while the uncomfortable wind zone (especially those with wind speed > 1.75 m/s) gradually decreases.

The simulated indoor wind environment for Cases 5 to 8 is summarized in Table 4. As the Yinyan’s overhang length varies, the maximum wind speed on the 1.1 m evaluation plane ranges from 2.25 to 2.28 m/s, while the minimum wind speed ranges from 0.024 to 0.035 m/s. The differences in both maximum and minimum values are relatively small. On the 1.7 m evaluation plane, the maximum wind speed ranges from 2.17 to 2.21 m/s, and the minimum wind speed ranges from 0.007 to 0.024 m/s. There is a slight variation in the maximum and minimum wind speed from

Case 5 to Case 8. This indicates a weak correlation between the changes in Yinyan’s overhang length and the indoor wind speeds.

For Cases 5–8, the average wind speed on the 1.1 m evaluation plane ranges from 0.69 to 0.74 m/s, while on the 1.7 m evaluation plane, it ranges from 0.74 to 0.75 m/s. As the Yinyan’s overhang length increases, the indoor average wind speed on the 1.1 m evaluation plane gradually decreases. While the average wind speed on the 1.7 m evaluation plane remains relatively unchanged.

As the Yinyan’s overhang length varies, the ratios of comfortable and uncomfortable wind zones for both evaluation planes in Cases 5–8 show noticeable changes. As shown in Table 4, when Yinyan’s overhang length is 0.96 m (Case 5), the comfortable wind zone ratio on the 1.1 m evaluation plane is 59.99%, and the uncomfortable wind zone ratio is 20.45%. As the Yinyan’s overhang length increases, compared to Case 5, the comfortable wind zone ratio for Cases 6, 7, and 8 increases by approximately 1.94%, 4.28%, and 2.1%, respectively, while the uncomfortable wind zone ratio decreases by about 2.22%, 4.84% and 3.48%. Among these, Case 7 shows the largest increase in the comfortable speed zone ratio and the largest decrease in the uncomfortable wind zone ratio.

On the 1.7 m evaluation plane, as the Yinyan’s overhang length increases, the comfortable wind zone ratio decreases by approximately 1.77% in Case 6 and 0.10% in Case 8 compared to Case 5, while Case 7 shows a slight increase of 0.41%. Additionally, the uncomfortable wind zone ratio is significantly reduced in Case 6 by about 4.46%, while smaller reductions are also observed in Case 7 (1.81%) and Case 8 (1.65%).

To summarize, when the “Yinyan” is installed above the window frame, variations in its overhang length have little effect on the maximum and minimum indoor wind speeds. However, as the overhang length increases, the comfortable wind zone ratio increases on both evaluation planes, while the uncomfortable wind zone ratio decreases. The best indoor wind environment can be achieved when the Yinyan’s overhang length is 1.28 m (Case 7). The quality of the indoor wind environment is relatively poor when the Yinyan’s overhang length is 0.96 m (Case 5).

Influence of Yinyan’s position on the indoor wind environment under the same overhang length

Figure 14 compares indoor wind speeds when Yinyan is installed at the eaves and those when Yinyan is installed above the window frame, with an identical overhang length. The difference in maximum wind speed values is small and positive, indicating that the maximum wind speed is slightly higher when the “Yinyan” is installed at the eaves. The difference in minimum wind speed values is also small, with both positive and negative values, suggesting that Yinyan’s position has a minimal and irregular effect on the minimum wind speeds. Regarding the comparison of average wind speeds, the difference in indoor average wind speed is positive, ranging from 0.15 to 0.18 m/s, indicating that the average indoor wind speed is higher when the “Yinyan” is installed at the eaves.

Figure 15 compares comfortable and uncomfortable wind zone ratios for Yinyan, with identical overhang lengths, being installed at the eaves and above the window frame. As shown in Fig. 15a), the difference in the uncomfortable wind zone ratio on the 1.1 m evaluation plane is positive, while the difference in the comfortable wind zone ratio is negative. Nevertheless, as shown in Fig. 15b), the statistical results for the 1.7 m evaluation

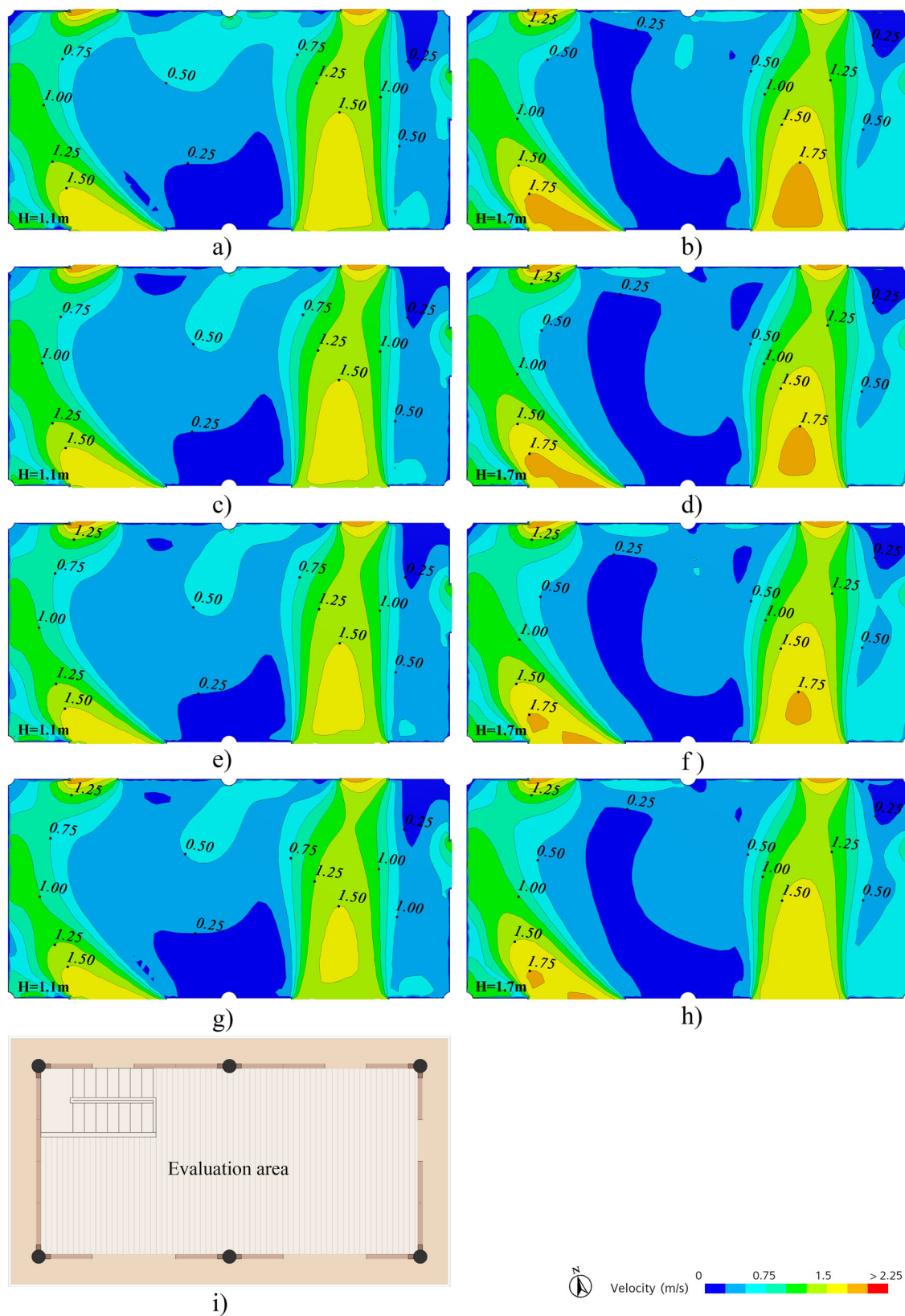


Fig. 13 | Indoor wind speed contour plots under different scenarios. a Case 5, 1.1 m evaluation plane; b Case 5, 1.7 m evaluation plane; c Case 6, 1.1 m evaluation plane; d Case 6, 1.7 m evaluation plane; e Case 7, 1.1 m evaluation plane; f Case 7,

1.7 m evaluation plane; g Case 8, 1.1 m evaluation plane; h Case 8, 1.7 m evaluation plane; i The 2nd floor plan of the tavern.

Table 4 | Indoor wind conditions with Yinyan installed above the window frame

	1.1 m evaluation plane					1.7 m evaluation plane				
	Wind speed (m/s)			Wind zone ratios		Wind speed (m/s)			Wind zone ratios	
	Max	Min	Avg.	Comfortable	Uncomfortable	Max	Min	Avg.	Comfortable	Uncomfortable
Case 5	2.27	0.025	0.74	59.99%	20.45%	2.21	0.018	0.75	54.82%	28.74%
Case 6	2.28	0.030	0.71	61.93%	18.23%	2.20	0.007	0.74	53.05%	24.28%
Case 7	2.26	0.035	0.71	64.27%	15.61%	2.18	0.024	0.75	55.23%	26.93%
Case 8	2.25	0.024	0.69	62.09%	16.97%	2.17	0.021	0.74	54.72%	27.09%

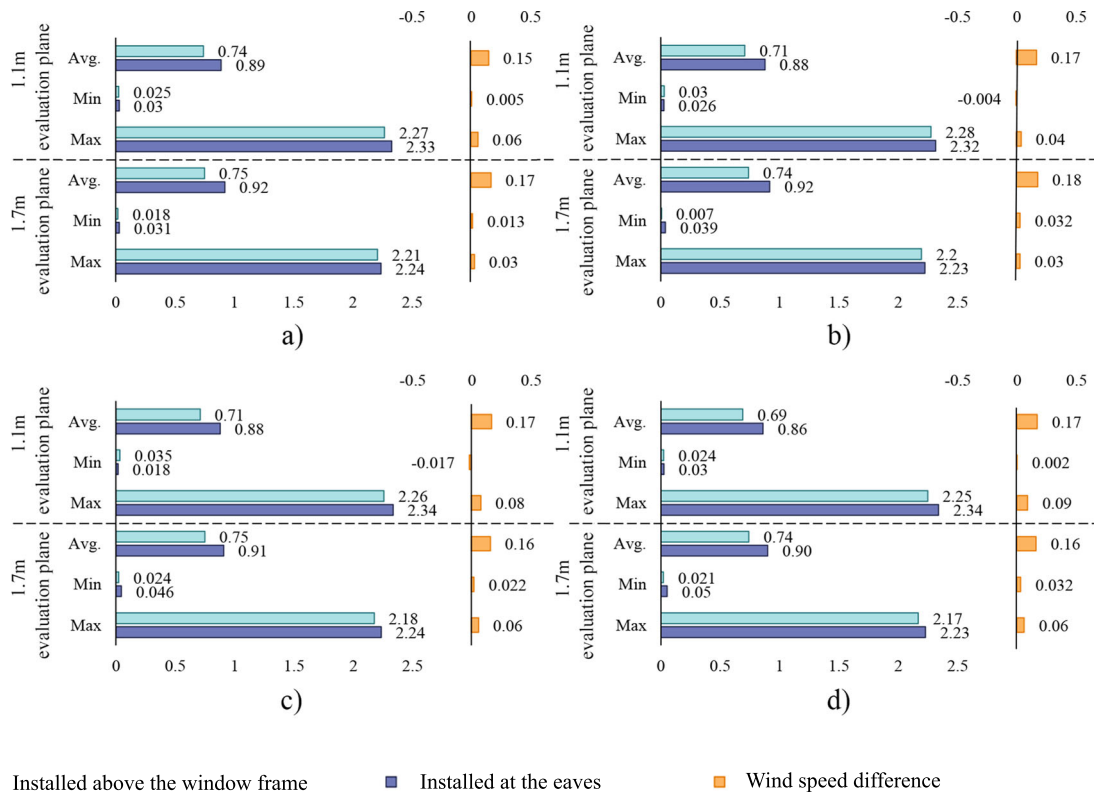


Fig. 14 | Comparison of indoor wind speeds for Yinyan, with identical overhang lengths, being installed at the eaves and above the window frame. a Yinyan width = 0.96 m (Case 1 and Case 5); **b** Yinyan width = 1.12 m (Case 2 and Case 6); **c** Yinyan width = 1.28 m (Case 3 and Case 7); **d** Yinyan width = 1.44 m (Case 4 and Case 8).

plane are the opposite, with the difference in the uncomfortable wind zone ratio being negative and the difference in the comfortable wind zone ratio being positive, which complicates the comparative analysis. The comparison of the mean values is shown in Fig. 15c).

From the comparison of the averages, when the Yinyan’s overhang length is 0.96 m, the difference in the comfortable wind zone ratio is positive, though small (0.14%), while the difference in the uncomfortable wind zone ratio is negative, reaching -2.81% . This suggests that with a Yinyan’s overhang length of 0.96 m installed at the eaves, the quality of the indoor wind environment is slightly better. When the overhang length of Yinyan is increased to 1.12 m, the difference in the comfortable wind zone ratio remains slightly positive (0.14%), while the difference in the uncomfortable wind zone ratio becomes positive as well (0.57%). This indicates that a 1.12 m long Yinyan installed above the window frame would be able to offer a marginal improvement on the indoor wind environment. When the Yinyan’s overhang lengths are 1.28 m, and 1.44 m, the difference in the comfortable wind zone ratios is negative (-2.23% , and -1.3%), and the difference in the uncomfortable wind zone ratios is positive (0.66%, and 0.26%), indicating that Yinyan with these overhang lengths, when installed above

the window frame, result in a relatively better indoor wind environment quality.

To summarize, the position of the “Yinyan” has a minimal impact on both the maximum and minimum indoor wind speeds, though it does have some effect on the average wind speeds. When the “Yinyan” is installed at the eaves, the indoor average wind speed is higher. Considering both the comfortable and uncomfortable wind zone ratios, when Yinyan is installed at the eaves and its overhang length is 0.96 m, the indoor wind environment quality is slightly better. When Yinyan is installed above the window frame and its overhang lengths are 1.12 m, 1.28 m, or 1.44 m, the indoor wind environment quality is relatively better.

Discussion

The painters in the Song Dynasty demonstrated a systematic understanding of architectural design and construction. As a result, buildings depicted in “Wumu” paintings are precisely detailed, with standardized and accurate proportions^{54,55}. By integrating “Wumu” paintings with the then building construction guide, it is possible to rebuild mock-ups for buildings from the Song Dynasty, consistent with the methodologies and conclusions proposed by Chiu et al. and Dong^{28,30}. In this study, the *Life along the Bian River at the*

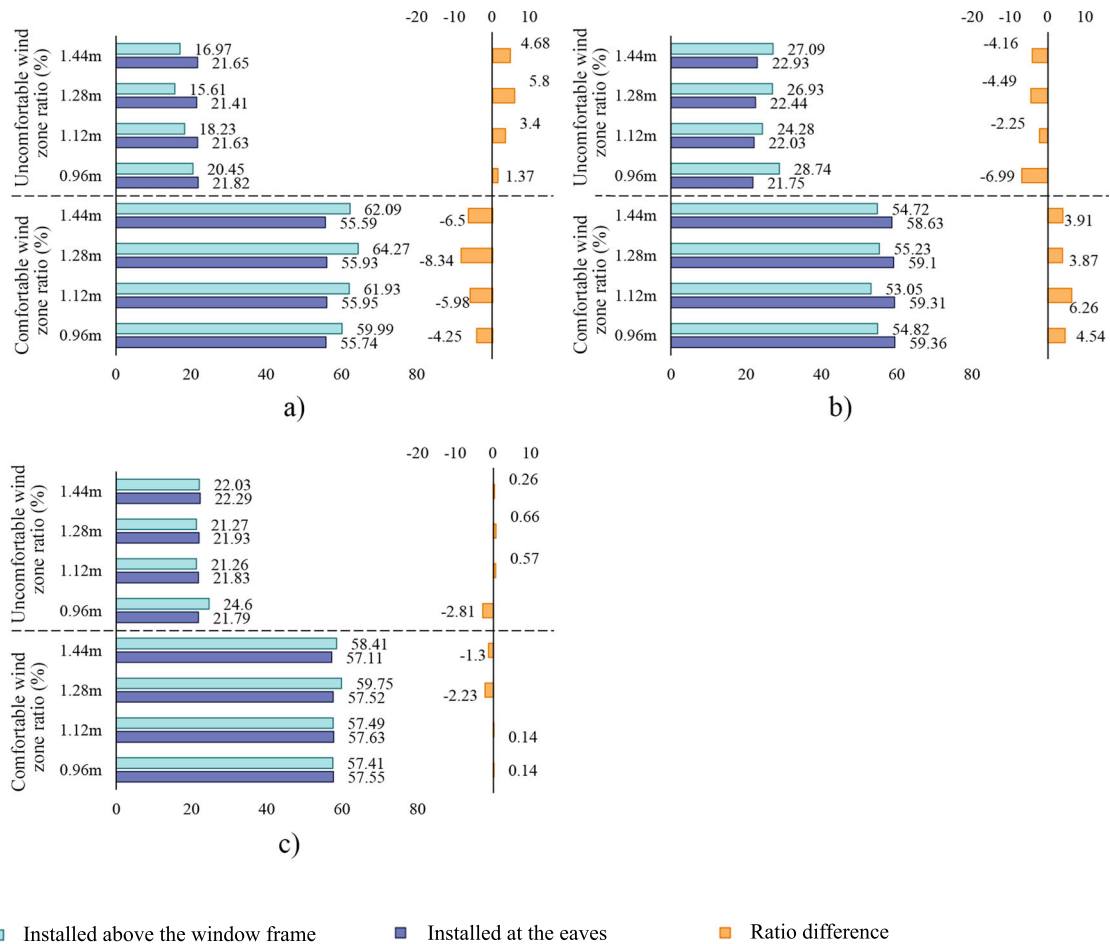


Fig. 15 | Comparison of comfortable and uncomfortable wind zone ratios for Yinyan, with identical overhang lengths, being installed at the eaves and above the window frame. a 1.1 m evaluation plane; **b** 1.7 m evaluation plane; **c** Average values for the 1.1 m and 1.7 m evaluation planes.

Qing Ming Festival and *Yingzao Fashi* have been used as key references for developing a digital model of the two-story building. Integrating paintings of the Song Dynasty into architectural research helps address the scarcity of well-preserved building heritage from that period and provides essential information for the digital represervation of Song architecture. Furthermore, this approach emphasizes not only the cultural and artistic values of paintings from the Song Dynasty, but also their academic significance. The elements depicted in these paintings (e.g., architecture and clothing) serve as important visual documents for examining the social and historical development of the Song Dynasty.

The building component “Yinyan” examined in this study features flexible installation options. When installed at the eaves, it functions as an extension of the roof. Previous studies have shown that roof geometry significantly influences indoor natural ventilation, and the pitch of the roof also plays a role^{56,57}. Tominaga et al. found that a roof pitch of 15° caused no significant change in pressure difference between the windward and leeward sides of a building, while a 30° pitch led to an increased pressure difference⁵⁸. Peren et al. demonstrated that a 45° roof pitch significantly enhances indoor airflow volume⁵⁹. In their experiments on eaves, they further observed that windward eaves improved ventilation more effectively than leeward ones. The most favorable ventilation performance was achieved when the windward eaves were set at 27° (aligned with the roof pitch) and the leeward eaves at 90°⁶⁰. In the present study, the “Yinyan” forms an angle of approximately 20° with the horizontal plane. Analysis of both vertical airflow and indoor wind speed distribution indicates that its impact on overall ventilation is limited, consistent with previous findings. However, it does influence the ratios of comfortable and uncomfortable wind zones. When installed above the window frame, the “Yinyan” exerted a greater impact on

indoor airflow, leading to more notable changes in the comfortable and uncomfortable wind zone ratios.

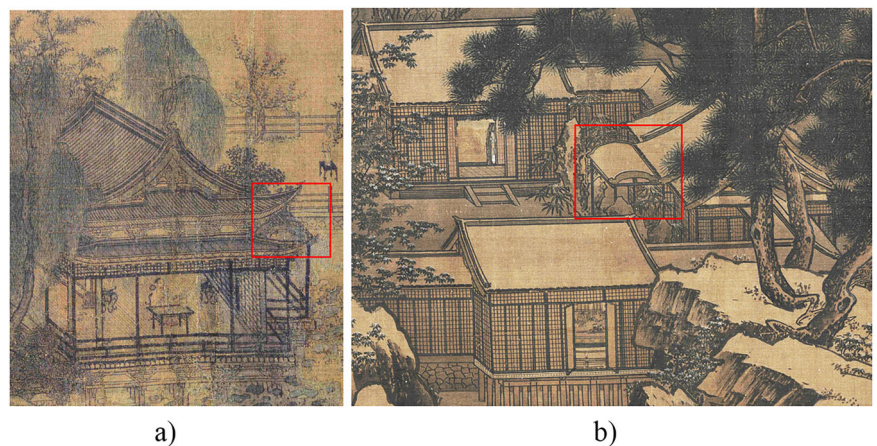
The statistical results of 8 cases are summarized in Table 5. When the “Yinyan” is installed at the eaves (Cases 1–4), the comfortable wind zone ratio on the 1.1 m evaluation plane initially increases and then decreases following the increasing of its overhang length, with Case 2 showing the highest ratio. Conversely, the uncomfortable wind zone ratio first decreases and then increases, reaching its lowest value in Case 3. On the 1.7 m evaluation plane, the comfortable wind zone ratio gradually decreases, while the uncomfortable wind zone ratio increases as the overhang length of Yinyan increases. Based on the mean values from both evaluation planes, the indoor wind environment quality is relatively better when the Yinyan’s overhang length is 1.12 m (Case 2), whereas it is slightly worse when the Yinyan’s overhang length is 1.44 m (Case 4).

When the “Yinyan” is installed above the window frame (Cases 5–8), the comfortable wind zone ratio on the 1.1 m evaluation plane initially increases and then decreases following the increasing of its overhang length, reaching the highest value in Case 7. Conversely, the uncomfortable wind zone ratio first decreases and then increases, with Case 7 showing the lowest value. On the 1.7 m evaluation plane, Case 7 also exhibits the highest comfortable wind zone ratio, while Case 6 shows the lowest uncomfortable wind zone ratio. Based on the mean values from both evaluation planes, the indoor wind environment quality is relatively better when the Yinyan’s overhang length is 1.28 m (Case 7), whereas it is slightly worse when the Yinyan’s overhang length is 0.96 m (Case 5). Out of the 8 cases, Case 7 demonstrates the best indoor wind environment, while Case 5 shows the worst case scenario. This indicates that, in Kaifeng City and other cities under similar climatic conditions,

Table 5 | Comfortable and uncomfortable wind zone ratios for Yinyan with different overhang lengths and installation positions

Installation Position	Case	1.1 m evaluation plane		1.7 m evaluation plane		Mean value	
		comfortable wind zone ratio	uncomfortable wind zone ratio	comfortable wind zone ratio	uncomfortable wind zone ratio	comfortable wind zone ratio	uncomfortable wind zone ratio
Installed at the eaves	Case 1	55.74%	21.82%	59.36%	21.75%	57.55%	21.79%
	Case 2	55.95%	21.63%	59.31%	22.03%	57.63%	21.83%
	Case 3	55.93%	21.41%	59.10%	22.44%	57.52%	21.93%
	Case 4	55.59%	21.65%	58.63%	22.93%	57.11%	22.29%
Installed above the window frame	Case 5	59.99%	20.45%	54.82%	28.74%	57.41%	24.60%
	Case 6	61.93%	18.23%	53.05%	24.28%	57.49%	21.26%
	Case 7	64.27%	15.61%	55.23%	26.93%	59.75%	21.27%
	Case 8	62.09%	16.97%	54.72%	27.09%	58.41%	22.03%

Fig. 16 | Evolution of the Yinyan in partial views of Song Dynasty paintings. a *Enjoying the Cold Air in Pavilion over water*; **b** *Four Seasons*.



installing “Yinyan” above the window frame in traditional buildings would significantly improve the indoor wind environment. An appropriate overhang length can enhance the indoor wind environment. For small-scale traditional buildings with 2-3 standard rooms, installing a Yinyan with an overhang length of 1.28 m (equal to 4 chi) above the window frame would result in a relatively better indoor wind environment. These insights offer scientific and quantitative evidence for the multisensory digital representation of historical architecture in Kaifeng back to the Song Dynasty, as well as for the development of eco-design educational practices rooted in traditional wisdom.

In Lin’an (current Hangzhou City) during the Southern Song Dynasty, where rainfall was frequent, people desired more sheltered exterior spaces for outdoor activities even in raining days. As a result, the “Yinyan” gradually extended outward and was supported by additional columns, eventually evolving into an exterior corridor or “Xuan” (a.k.a. a covered exterior corridor with an arched roof). This evolution can be seen in paintings of the Southern Song Dynasty, such as *Enjoying the Cold Air in Pavilion over water* (*Shui Ge Na Liang Tu* in Pinyin) and *Four Seasons* (*Si Jing Shan Shui Tu* in Pinyin) (Fig. 16)^{29,61}. These examples demonstrate how, in response to the regional microclimatic conditions, the “craftsmen/architects” in the Song Dynasty adapted the form and size of “Yinyan” (and other climate-responsive architectural components) to create more comfortable built environments. The wisdom of climate-sensitive environmental designs has been properly recorded and inherited in Song Dynasty paintings. When digitally reconstructing and representing the architectural heritage of the Song Dynasty, such human-centered design wisdom from historical paintings, as reflected in the adaptable and personalized building component “Yinyan”, should be taken into account. Adjusting the form and sizes of

climate-responsive components in accordance with environmental and climatic conditions not only enhances the accuracy of digital representation but also ensures the faithful transmission of traditional design thinking and the relevant architectural knowledge. This approach provides a solid technical foundation for the conservation and restoration of Song architecture. Furthermore, by integrating the climate-adaptive design wisdom embedded in Song paintings with modern technologies and materials, it is possible to apply these principles to contemporary architecture. Such practices not only represent an innovative approach to cultural heritage transmission but also offer valuable contributions to the sustainable development of today’s human settlements.

This study presents a preliminary analysis on how the position and sizes of the “Yinyan” influence the indoor wind environment in the traditional architecture of the Kaifeng region, using a digital mock-up derived from *Life along the Bian River at the Qing Ming Festival*. However, since the digital representation is based on a historical painting, certain inaccuracies may exist. Additionally, the simulation is conducted under contemporary climate conditions, which differ from those in Song Dynasty. These result in certain limitations of the study. Future research will incorporate more preserved Song architectural heritages to enhance the reliability of digital representation and will explore a wider range of climate scenarios and external configurations to further develop the theoretical framework of climate-responsive design in traditional architecture. Moreover, as the “Yinyan” affects not only ventilation but also other aspects such as indoor daylighting and solar gains, future research needs to explore the combined effects of “Yinyan”, aiming to offer a more comprehensive theoretical foundation for the multisensory digital representation of architectural heritage.

Data availability

The datasets used and analyzed in the current study are available from the corresponding authors upon reasonable request.

Received: 19 June 2025; Accepted: 27 January 2026;

Published online: 04 February 2026

References

- Li, Y. et al. A review of the tools and techniques used in the digital preservation of architectural heritage within disaster cycles. *Herit. Sci.* **11**, 199 (2023).
- Santana Quintero, M. Background, role and challenge of digitalization of architectural heritage. *Estoa* **2**, 7–21 (2013).
- Zhang, K. & Fassi, F. Transforming Architectural Digitisation: Advancements in AI-Driven 3D Reality-Based Modelling. *Heritage* **8**, 81 (2025).
- Arrighi, G., See, Z. S. & Jones, D. Victoria Theatre virtual reality: A digital heritage case study and user experience design. *Digit. Appl. Archaeol. Cult. Herit.* **21**, e00176 (2021).
- Bozzelli, G. et al. An integrated VR/AR framework for user-centric interactive experience of cultural heritage: The ArkaeVision project. *Digit. Appl. Archaeol. Cult. Herit.* **15**, e00124 (2019).
- De Fino, M., Ceppi, C. & Fatiguso, F. Virtual tours and informational models for improving territorial attractiveness and the smart management of architectural heritage: The 3D-IMP-ACT project. *Int. Arch. Photogramm. Remote Sens. Spat. Inf. Sci.* **XLIV-M-1-2020**, 473–480 (2020).
- Ong, C.-E. & Jin, G. Simulacra and simulation: double simulation at a North Song Dynasty theme park. *Tour. Geogr.* **19**, 227–243 (2017).
- de Pee, C. Wards of Words: Textual Geographies and Urban Space in Song-Dynasty Luoyang, 960–1127. *J. Econ. Soc. Hist. Orient.* **52**, 85–116 (2009).
- Liu, X. *Research on Ecological Concept of Architecture and Environment in the Ruled-line paintings of Song Dynasty (in Chinese)*. Master's thesis (Hunan University, 2019).
- Zhou, Y., Zhang, M., Li, L. & Huang, W. Parametric 3D reconstructing and interpreting iconographic evidence: case of the Song Dynasty architectural massing typologies. *Herit. Sci.* **13**, 300 (2025).
- Yao, X., Hu, L. & Zhang, J. Reconstructing the local structures of Chinese ancient architecture using unsupervised depth estimation. *Herit. Sci.* **12**, 318 (2024).
- Valenti, R. M. F., Aliano, C. L., Paternò, E. M. & Gazzè, E. Silent Cultural Heritage: Digitalization of the Archaeological Artefacts of Santa Lucia di Mendola for an Interdisciplinary Reconstruction. *SCIRES-IT* **11**, 179–194 (2021).
- Massafra, A., Costantino, C., Predari, G. & Gulli, R. Building Information Modeling and Building Performance Simulation-Based Decision Support Systems for Improved Built Heritage Operation. *Sustainability* **15**, 11240 (2023).
- Song, H., Selim, G. & Gao, Y. Smart Heritage Practice and Its Characteristics Based on Architectural Heritage Conservation-A Case Study of the Management Platform of the Shanghai Federation of Literary and Art Circles China. *Sustainability* **15**, 16559 (2023).
- De Fino, M., Bruno, S. & Fatiguso, F. Dissemination, Assessment and Management of Historic Buildings by Thematic Virtual Tours and 3D Models. *Virtual Archaeol. Rev.* **13**, 88–102 (2022).
- Nguyen, T. A., Do, S. T., L.-H., L., Nguyen, V. T. & T.-A., P. Practical workflow for cultural heritage digitalization and management: a case study in Vietnam. *Int. J. Constr. Manag.* **23**, 2305–2319 (2023).
- Milic, R. J., McPherson, P., McConchie, G., Reutlinger, T. & Singh, S. Architectural history and sustainable architectural heritage education: digitalisation of heritage in New Zealand. *Sustainability* **14**, 16432 (2022).
- Yang, N., Chen, B. & Xi, J. A theoretical design framework of contemporary vernacular architecture based on a scoping review of the best practices worldwide. *Buildings* **14**, 3525 (2024).
- Gou, S., Li, Z., Zhao, Q., Nik, V. M. & Scartezzi, J.-L. Climate responsive strategies of traditional dwellings located in an ancient village in hot summer and cold winter region of China. *Build. Environ.* **86**, 151–165 (2015).
- Mohammadi, A., Saghafi, M. R., Tahbaz, M. & Nasrollahi, F. The study of climate-responsive solutions in traditional dwellings of Bushehr City in Southern Iran. *J. Build. Eng.* **16**, 169–183 (2018).
- Iravani, I., Etessam, H., Masoud, M. & Mofidi, S. M. The role of wind and natural ventilation in the vernacular architecture of Zavareh. *Int. J. Vent.* **8**, 175–186 (2016).
- Ryu, Y., Kim, S. & Lee, D. The influence of wind flows on thermal comfort in the Daechung of a traditional Korean house. *Build. Environ.* **44**, 18–26 (2009).
- Chen, H. & Zhang, X. Research and simulation of traditional settlement wind and heat environment based on computer intelligent computing technology. *Comput. Intell. Neurosci.* **2022**, 3715730 (2022).
- Aydin, Y. C. & Mirzaei, P. A. Wind-driven ventilation improvement with plan typology alteration: A CFD case study of traditional Turkish architecture. *Build. Simul.* **10**, 239–254 (2017).
- Suleiman, S. & Himmo, B. Direct comfort ventilation. Wisdom of the past and technology of the future (wind-catcher). *Sustain. Cities Soc.* **5**, 8–15 (2012).
- Mailleur, S. & Saleri, R. Imagining Roman port cities: from iconographic evidence to 3D reconstruction. In *Beyond digital representation: advanced experiences in AR and AI for cultural heritage and innovative design* (eds. Giordano, A., Russo, M. & Spallone, R.) 279–290 (Springer, 2023).
- Yu, M., Li, C. & Chen, S. Research on the Architectural Drafting Features in the Song and Yuan Dynasties in Light of the Angle Design of the Ruler Painting (in Chinese). *J. Xi' Univ. Archit. Technol. (Soc. Sci. Ed.)* **42**, 14–20 (2023).
- Chiu, Y.-H., Wang, C.-C. & Tsai, C.-Y. The discussion on the mystery season of a historical painting “Qing Ming Shang He Tu” by the thermal comfort analysis method. *Build. Simul.* **12**, 299–312 (2018).
- Zhejiang University Center for the Study of Ancient Chinese Painting and Calligraphy. *Complete Collection of Song Paintings (Volume 1)* (in Chinese) (Zhejiang University Press, 2010).
- Dong, B. *Study on the Restoration Design of Song Pavilions and Buildings Based on the Regime of Large Wood Structures in Building Methods in the Song Dynasty* (in Chinese). Master's thesis (Tsinghua University, 2014).
- Li, J. *Yingzao Fashi* (in Chinese) (China Architecture & Building Press, 2006).
- Zhou, H. *Qingbo Biezhì* (in Chinese) (Elephant Press, 2012).
- Zheng, Q. The research of the evolution of the spatial boundaries of the Literati's residential and recreational buildings in the Song Dynasty based on the comparative study of architectures in Song Dynasty paintings (in Chinese). *Archit. J.* **52**, 170–175 (2021).
- Zhejiang University Center for the Study of Ancient Chinese Painting and Calligraphy. *Complete Collection of Song Paintings (Volume 3)* (in Chinese) (Zhejiang University Press, 2015).
- Liu, D. *History of Ancient Chinese Architecture* (in Chinese) (China Architecture & Building Press, 1984).
- Ding, D., Yu, X. & Wang, Z. The Evolution of the Living Environment in Suzhou in the Ming and Qing Dynasties Based on Historical Paintings. *ACM J. Comput. Cult. Herit.* **14**, 1–14 (2021).
- Wang, G. Discussion on the Series of Different Bay Width Ratios in the Plan and Elevation Proportions of Tang and Song Dynasty Buildings (in Chinese). *Archit. Hist.* **3**, 12–25 (2003).
- Liang, S. *Yingzao Fashi with Annotations* (in Chinese) (China Architecture & Building Press, 1983).

39. Tominaga, Y. et al. AIJ guidelines for practical applications of CFD to pedestrian wind environment around buildings. *J. Wind Eng. Ind. Aerodyn.* **96**, 1749–1761 (2008).
40. Zhang, H., Xiong, M., Chen, B. & Wang, Y. Influence of tropical cyclones on outdoor wind environment in high-rise residential areas in Zhejiang Province, China. *Sustainability* **14**, 3932 (2022).
41. Ricci, A. & Blocken, B. On the reliability of the 3D steady RANS approach in predicting microscale wind conditions in seaport areas: The case of the IJmuiden sea lock. *J. Wind Eng. Ind. Aerodyn.* **207**, 104437 (2020).
42. Brozovsky, J., Simonsen, A. & Gaitani, N. Validation of a CFD model for the evaluation of urban microclimate at high latitudes: A case study in Trondheim, Norway. *Build. Environ.* **205**, 108175 (2021).
43. Schatzmann, M., Olesen, H. & Franke, J. *COST 732 Model Evaluation Case Studies: Approach and Results* (COST Office, 2010).
44. Ministry of Housing and Urban-Rural Development of the People's Republic of China. *Load code for the design of building structures (GB 50009-2012)* (China Architecture & Building Press, 2012).
45. Yang, W. & Zhang, G. Thermal comfort in naturally ventilated and air-conditioned buildings in humid subtropical climate zone in China. *Int. J. Biometeorol.* **52**, 385–398 (2008).
46. ANSI/ASHRAE. *Thermal Environmental Conditions for Human Occupancy* (Standard 55-2023). <https://www.ashrae.org/> (2023).
47. Ministry of Housing and Urban-Rural Development of the People's Republic of China. *Evaluation standard for indoor thermal environment in civil buildings (GB/T 50785-2012)* (China Standards Press, 2012).
48. Rupp, R. F., Vásquez, N. G. & Lamberts, R. A review of human thermal comfort in the built environment. *Energy Build* **105**, 178–205 (2015).
49. Zhu, Y., Luo, M., Ouyang, Q., Huang, L. & Cao, B. Dynamic characteristics and comfort assessment of airflows in indoor environments: A review. *Build. Environ.* **91**, 5–14 (2015).
50. Su, X., Zhang, X. & Gao, J. Evaluation method of natural ventilation system based on thermal comfort in China. *Energy Build* **41**, 67–70 (2009).
51. Gong, N. et al. The acceptable air velocity range for local air movement in the tropics. *HVACR Res* **12**, 1065–1076 (2011).
52. Wang, C., Jin, M. & Cheng, H. Influence of deflectors on indoor airflow velocity distribution under natural ventilation conditions. *Front. Energy Res.* **12**, 1327577 (2024).
53. Cândido, C., de Dear, R., Lamberts, R. & Bittencourt, L. Natural ventilation and thermal comfort: air movement acceptability inside naturally ventilated buildings in the Brazilian hot humid zone. In: *Air Conditioning and the Low Carbon Cooling Challenge*. (Network for Comfort and Energy Use in Buildings, 2008).
54. Li, Z. *Deyu Zhai Huapin* (in Chinese) (Beifang Literature & Art Publishing House, 2021).
55. Guo, R. *Tuhua Jianwen Zhi* (in Chinese) (Zhonghua Book Company, 1985).
56. Peren, J. I., van Hooff, T., Ramponi, R., Blocken, B. & Leite, B. C. C. Impact of roof geometry of an isolated leeward sawtooth roof building on cross-ventilation: Straight, concave, hybrid or convex? *J. Wind Eng. Ind. Aerodyn.* **145**, 102–114 (2015).
57. Kindangen, J., Krauss, G. & Depecker, P. Effects of roof shapes on wind-induced air motion inside buildings. *Build. Environ.* **32**, 1–11 (1997).
58. Tominaga, Y., Zhang, X. & Miyakoshi, K. Wind tunnel experiment on cross-ventilation of generic isolated building with various roof shapes: Impact of roof pitch and eaves. *Build. Environ.* **265**, 111974 (2024).
59. Perén, J. I., van Hooff, T., Leite, B. C. C. & Blocken, B. CFD analysis of cross-ventilation of a generic isolated building with asymmetric opening positions: Impact of roof angle and opening location. *Build. Environ.* **85**, 263–276 (2015).
60. Perén, J. I., van Hooff, T., Leite, B. C. C. & Blocken, B. Impact of eaves on cross-ventilation of a generic isolated leeward sawtooth roof building: Windward eaves, leeward eaves and eaves inclination. *Build. Environ.* **92**, 578–590 (2015).
61. Zhejiang University Center for the Study of Ancient Chinese Painting and Calligraphy. *Complete Collection of Song Paintings (Volume 2)* (in Chinese) (Zhejiang University Press, 2010).

Acknowledgements

This work was supported by Zhejiang University Center for Chinese Painting and Calligraphy, the Zhejiang Provincial Philosophy and Social Sciences Planning Project (Grant no. 25NDJC018YBM), Xi'an Jiaotong-Liverpool University Research Development Fund (Grant no. RDF-20-02-19), and the Technical Service Project committed by Suzhou Industrial Park Planning and Construction Committee (Grant no. RDH10120240159). The authors would like to thank the editor and anonymous reviewers for their support in improving the quality of this manuscript.

Author contributions

Hua Zhang: Writing – original draft, Software, Validation, Methodology, Data analysis. Minghui Xiong: Writing – review & editing, Data curation, Resources. Bing Chen: Writing – review & editing, Supervision, Resources. Kaiguo Si: Conceptualization. Jialong Lai: Investigation.

Competing interests

The authors declare no competing interests.

Additional information

Correspondence and requests for materials should be addressed to Minghui Xiong or Bing Chen.

Reprints and permissions information is available at <http://www.nature.com/reprints>

Publisher's note Springer Nature remains neutral with regard to jurisdictional claims in published maps and institutional affiliations.

Open Access This article is licensed under a Creative Commons Attribution-NonCommercial-NoDerivatives 4.0 International License, which permits any non-commercial use, sharing, distribution and reproduction in any medium or format, as long as you give appropriate credit to the original author(s) and the source, provide a link to the Creative Commons licence, and indicate if you modified the licensed material. You do not have permission under this licence to share adapted material derived from this article or parts of it. The images or other third party material in this article are included in the article's Creative Commons licence, unless indicated otherwise in a credit line to the material. If material is not included in the article's Creative Commons licence and your intended use is not permitted by statutory regulation or exceeds the permitted use, you will need to obtain permission directly from the copyright holder. To view a copy of this licence, visit <http://creativecommons.org/licenses/by-nc-nd/4.0/>.

© The Author(s) 2026